國 立 中 央 大 學

機械工程研究所

碩/博士論文

模版 ncuthesisCJK 使用說明

An example in LaTeX/XeLaTeX

研究生: 羅吉昌

指導教授: 羅吉昌

共同指導: 甲教授
乙教授

中 華 民 國 一百零二 年 六 月

國 立 中 央 大 學

機械工程研究所

碩/博士論文

模版 ncuthesisCJK 使用說明

An example in LaTeX/XeLaTeX

研究生: 羅吉昌

指導教授: 羅吉昌

共同指導: 甲教授
乙教授

中 華 民 國 一百零二 年 六 月

國立中央大學圖書館
碩博士論文電子檔授權書

(101 年 9 月最新修正版)

本授權書授權本人撰寫之碩/博士學位論文全文電子檔(不包含紙本、詳備註 1 說明)，在「國立中央大學圖書館博碩士論文系統」。(以下請擇一勾選)

(　　)**同意** (立即開放)

(　　)**同意** (請於西元 _____年_____月_____日開放)

(　　)**不同意**，原因是：_____

在國家圖書館「臺灣博碩士論文知識加值系統」

(　　)**同意** (立即開放)

(　　)**同意** (請於西元 _____年_____月_____日開放)

(　　)**不同意**，原因是：_____

以非專屬、無償授權國立中央大學、台灣聯合大學系統圖書館與國家圖書館，基於推動「資源共享、互惠合作」之理念，於回饋社會與學術研究之目的，得不限地域、時間與次數，以紙本、微縮、光碟及其它各種方法將上列論文收錄、重製、與利用，並得將數位化之上列論文與論文電子檔以上載網路方式，提供讀者基於個人非營利性質之線上檢索、閱覽、下載或列印。

研究生簽名: _____　　學號：_____

論文名稱:_____

指導教授姓名：_____

系所 ：_____所　☐博士班　☐碩士班

備註：

1. 本授權書之授權範圍僅限電子檔，紙本論文部分依著作權法第 15 條第 3 款之規定，採推定原則即預設同意圖書館得公開上架閱覽，如您有申請專利或投稿等考量，不同意紙本上架陳列，須另行加填聲明書，詳細說明與紙本聲明書請至 http://thesis.lib.ncu.edu.tw/ 下載。
2. 本授權書請填寫並**親筆**簽名後，裝訂於各紙本論文封面後之次頁（全文電子檔內之授權書簽名，可用電腦打字代替）。
3. 請加印一份單張之授權書，填寫並親筆簽名後，於辦理離校時交圖書館（以統一代轉寄給國家圖書館）。
4. 讀者基於個人非營利性質之線上檢索、閱覽、下載或列印上列論文，應遵守著作權法規定。

國立中央大學碩士班研究生

論文指導教授推薦書

_____學系/研究所_____研究生所提之論文

_____ 係由本

（題　　目）

人指導撰述，同意提付審查。

指導教授_____ (簽章)

____年____月____日

國立中央大學博士班研究生

論文口試委員審定書

_____學系/研究所_____研究生所提之論文

_____

經本委員會審議，認定符合博士資格標準。

學位考試委員會召集人 _____

委　　員 _____

_____

_____

_____

中 華 民 國　　年　　月　　日

模版 ncuthesisCJK 使用說明

An example in LaTeX/XeLaTeX

中文摘要

關鍵字： 碩博士論文，體裁檔，LaTeX，XeLaTeX

此論文範例得以完成是由於體裁檔(ncuthesis.cls)的完成。期間多方閱讀、吸收、漸有所獲，直至發掘兩篇網路文章，深入了解後再加入中文化及適當增修而成。本體裁檔可再增修，複製，直接採用做個人用途，或供單位使用，唯不可做商業用途。

此套件係自助編寫屬非賣品，可自由使用，但不做任何保證。期望提供學生便利性，做出符合國立中央大學所規範的研究所論文格式，但不隱含任何商業價值。Open NCU Thesis Requirements

來源

https://code.google.com/p/ncu-thesis-latex-template/

功能

- 論文格式滿足本校要求。
- Uncode/UTF8 中文化。
- 可選擇編譯方式(pdfLaTeX，XeLaTeX)。
- 可選單面印刷或雙面印刷。
- 快速編譯及越界偵錯。
- 可列印紙張結構及參數。
- 顯示智財權及製作日期。
- 具索引及浮水印功能。
- 其它文書製作及提醒功能。
- 如何使用體裁檔請看第一章說明。
- 如何使用LaTeX 請看第二章說明。
- 如何製作參考文獻請看第三章說明。

模版 ncuthesisCJK 使用說明

An example in LaTeX/XeLaTeX

英文摘要

Keywords: Master/Doctorial thesis, Class file, LaTeX, XeLaTeX

Source

https://code.google.com/p/ncu-thesis-latex-template/

Features

- Master/Doctorial thesis stipulated by National Central University.
- Unicode/UTF8 supports.
- Compilable by pdfLaTeX or XeLaTeX.
- Oneside or twoside printing.
- Fast compilation and overfull detection.
- Page layout and parameters.
- Copyright and time stamp.
- Index, watermark capabilities.
- Other thesis variants and todonote reminder.
- How to use this package –– Chapter 1.
- How to use LaTeX (very brief) –– Chapter 2.
- How to generate references –– Chapter 3.

模版 ncuthesisCJK 使用說明

An example in LaTeX/XeLaTeX

謝誌

體裁檔受啓發於兩位英美教授於網路上的文章，並經吾人中文化及適當增修而成。本體裁檔可再增修，複製，直接採用做個人用途，或單位使用，唯不可做商業用途。請尊重上述兩位教授的無私奉獻。

- 感謝TeX/LaTeX網路社群內，龐大的TeX/LaTeX社群及其網頁提供無價資訊。
- 欣逢中央大學教務處註冊組組長，蕭嘉璋老師，見微知著，並予協助，僅此誌謝。
- 承蒙太空及遙測研究中心蔡富安老師協助在Ubuntu 12.04上TeXLive-2009測試成功，僅此誌謝。
- 2013/06/13碩士班 葉信麟同學發現目錄頁碼不正確。
- 2013/07/04碩士班 林億同學發現附錄節碼不正確。

Contents

頁次

List of Figures

List of Tables


國立中央大學

Todo list

完稿時要用[disable]除去所有todos。


國立中央大學

模版 ncuthesisCJK 使用說明

An example in LaTeX/XeLaTeX

符號說明

\dept	: 研究所
\degree	: 碩/博士 or 專題研究 or 論文計畫書
\title	: 論文中文題目
\subtitle	: 論文英文題目
\logo	: 封面校徽(預設中央校徽)
\author	: 作者
\mprof	: 指導教授
\sprofi, \sprofii	: 兩位共同指導
\degreedate	: 中 華 民 國 XXX 年 X 月
\copyyear	: 著作完成年
\includepdf	: 插頁指令，需pdfpages巨集
\fontsize...\selectfont	: 設定字大小行距
\bookbone	: 書脊短時用
abstractcn	: 中文摘要環境名，檔案則爲abstractcn.tex
abstracten	: 中文摘要環境名，檔案則爲abstracten.tex
acknowledgements	: 謝誌環境名，檔案則爲acknowledge.tex
appendA	: 附錄一環境名，檔案則爲appendix.tex
appendB	: 附錄二環境名，檔案則爲appendix.tex
symbols	: 符號說明環境名，檔案則爲symbol.tex

1. Introduction

According to Hindu cosmological mythology, ancient people believe that a giant turtle bears the world on its back. Even after we stepped onto the moon at 1969, there are still plenty that we cannot explain. In the novel Lord of the Rings, the author named the path between hobbits as Mordor, which is also the name of the dark area on Pluto's moon, Charon. Recently, Mission New Horizons retrieved valuable data about Charon and Pluto. This thesis aims to explain the formation mechanisms of the red cap on the pole of Charon (fig. 1), especially during the long cold dark period, through observations in extreme ultra-violet (EUV) and vacuum ultra-violet (VUV) irradiation.

Composition of Charon

The main composition on the surface of Charon is H_2O. According to Infrared (IR) spectroscopy, it is a mixture of 90 % H_2O and 10 % tholin at millimetre depth. The second most dominant component is ammonia hydrate, which can be observed by earth-based telescopes (brown 2000, cook 2007). In far IR spectrum taken by LEISA camera on the New Horizons, concentrated ammonia is found on Organa crater (fig 2.) and throughout Charon (fig 3.) (Grundy 2016a). The third component which forms the dark red cap (tholin?) is cold-trapped methane from Pluto's atmosphere ejecta (Hoey 2017). The presence of nitrogen and other ejecta from Pluto are neglected in this thesis because according to the model of Hoey et al. (2017) (fig.4), during New horizons' approach, 98 % of the arrived ejecta is CH_4. Charon's atmospheric pressure is further constrained by New Horizons to be below 0.3 nano bars, which is 4×10^{-13} torr for all 14 atoms and molecules including CO, H_2, CH_4, Ne, Ar, etc. (fig. 5). CH_4 remains undetectable when we convert the momentum of CH_4 with 7 hops on the surface of Charon until deposited onto cold enough part is 1×10^{-11} Pa, which is 7.5×10^{-14} torr (Grundy

2016b).

VUV irradiation

Ly-α appears to be the largest source in the dark side of Charon, with attributions from both solar occultation (70 %) and resonance scattering by atomic hydrogen flow (30 %) in the solar system at flux 3.5×10^7 photons cm^{-2} s^{-1} onto the winter pole of Charon (Grundy 2016b). The flux is 50 % larger than expected before Mission New Horizons (Gladstone 2015). CH_4 deposits at temperature below 25 K at pressure 7.4×10^{-14} torr. The time for depositing CH_4 is 2 times longer at the pole (130 earth years) than at 45 lattitude according to the thermal model of Grundy et al. (2016b) (fig 6). In order to understand the formation of tholin at different latitudes of Charon, we performed VUV irradiation on CH_4+NH_3 and CH_4+NH_3+H_2O experiments with different ratios (including 3:2, 1:5, 1:10 and 1:20 for CH_4+NH_3 and 5:3:4, 1:5:5 and 1:10:10 for CH_4+NH_3+H_2O ice mixtures) to simulate the conditions at different latitudes on Charon with base pressure $3times10^{-10}$ torr, simulating atmosphere on Charon at 15 K, which corresponds to temperature on Charon at winter times (Grundy 2016b) in interstellar processing system (IPS) (Chen 2014).

EUV irradiation

Apart from VUV irradiation, EUV irradiation also took part. VUV irradiation is believed to be the main process to convert CH_4 into heavier molecules which remained on the surface of Charon until the temperature of Charon become 60 K, at which methane evaporates from the ice. The ice is then further processed by EUV, solar wind, coronal mass ejections and interstellar pickup ions, etc to produce the tholin on Charon (Grundy 2016b). The EUV irradiation (>12.4 eV) is $8.7 \times 10^7 eV cm^{-2} s^{-1}$ at mean heliocentric distance 39 A.U. whereas VUV irradiation (Ly-α) is $1.9 \times 10^9 eV cm^{-2} s^{-1}$. In order to investigate the effectiveness of EUV to VUV irradiation, we kept temperature of CH_4+NH_3 (3:2 & 1:5) and CH_4+NH_3+H_2O (5:3:4) ice mixtures at 15 K and use the monochromatic 30.4 nm (He II) light provided by High flux beamline at National Synchrotron Radiation Research Centre (NSRRC) in Taiwan to irradiate the ice mixtures.

H_2O involved?

We compared the conditions of CH_4+NH_3 and CH_4+NH_3+H_2O because tholin on Titan is believed to be formed by CH_4+N_2 and a similar colour was observed on Charon. Charon is different from Titan as H_2O dominates on Charon. What are the differences between tholin formed by CH_4+NH_3 and CH_4+N_2? What role does H_2O play on Charon in the formation of tholin? Is it just diluting the formation or new compounds are formed?

In this thesis, we will introduce the formation reaction mechanisms of CH_4+NH_3 ice mixtures in EUV and VUV irradiation (section 3), the formation reaction mechanisms of CH_4+NH_3+H_2O ice mixtures in EUV and VUV irradiation (section 4), and the residues of these mixtures and a brief comparison with tholin on Titan will be made (section 5). With these results, we will have a better understanding about Charon and some astrophysical implications will be presented (section 6).


國立中央大學

2. Methods

2.1 Laboratory Astrophysics

To study the chemical reactivity in astrophysical environment experimentally, we conducted our experiments in Interstellar photoprocessing system (IPS) (Chen et al. 2014), an ultrahigh vacuum chamber with base pressure 3×10^{-10} torr and 14 K, corresponds to a density of 10^6 cm^{-3}, similar to dense cloud interiors. The system will be introduced in detail in section 2.1.1. To simulate the irradiation in interstellar environments, we use a micro-wave discharge hydrogen lamp (MDHL) and monochromatic extreme-ultraviolet irradiation (EUV) 30.4 nm to irradiate our ice mixtures, and they will be introduced in section 2.1.2 and 2.1.3 respectively. The experimental protocols will be elaborated in section 2.2. In order to better understand the physics behind, some basic theories of Infrared spectroscopy and concepts of chemical kinetics used in data analysis are included in section 2.3 and 2.4 respectively. To demonstrate the ice mixtures in KBOs, we used different configurations of ice mixtures that refers to different sections in chapter 3 and chapter 4.

2.1.1 Experimental simulations by IPS system

We conducted our astrophysical simulations studied in chapter 3 to 4 in Interstellar Photo Processing System (IPS) (figure 2.1). IPS consists in three systems: the main chamber, where our experiments take places; the detection system, where we collect our data; and a gasline system, where we prepare our samples.

The main system consists of an ultrahigh vacuum chamber equipped with a closed-cycle helium cryostat (CTI-M350). It is pumped by a turbo molecular pump (KTKT FF – 160/620ZE, capacity 600 liters s^{-1}), which is backed up by a scroll pump, and a non –evaporation get-

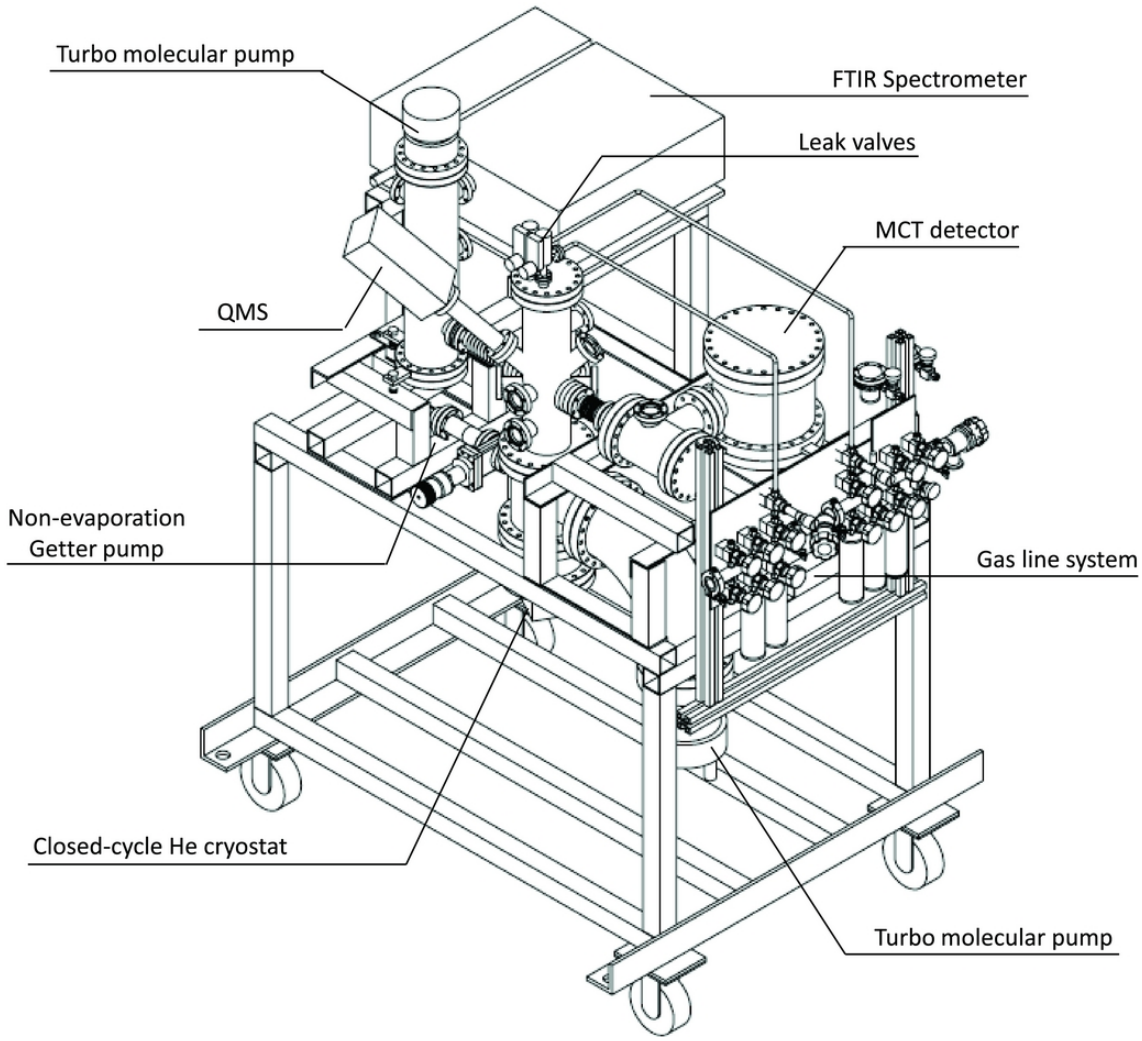

Figure 2.1: The schematic diagram of IPS system, mechanical pumps are not shown for clarity. (Quoted from Chen et al. 2014)

ter pump. The getter pump is a powerful tool to adsorb residue gases inside the main chamber, with a larger surface area, H_2, CO and N_2 are adsorbed to obtain a better base pressure. After baking, the base pressure of our main chamber can reach 1×10^{-10} torr at 14 K, monitored by a Granville-Phillips 370 Stabil-Ion gauge. This pressure can be used to demonstrate the dense cloud interior environments and star forming region. The substrate we have chosen is KBr, which can allow infra-red photons with 700 to 4000 cm^{-1} to penetrate. It is mounted by substrate holder made of oxygen-free copper, on the first stage of cold finger mounted on the tip of cryostat. Two silicon diodes and also a heater were placed onto the cold finger and one of the silicon diodes is near the substrate holder. They were connected to a temperature controller and PID system to achieve a warmup rate of 1K/min with an accuracy of 0.1 K.

The detection system consists in a mid-infrared Fourier transform spectrometer (mid-FTIR) (ABB FTLA2000-104) and a Quadrupole Mass Spectrometer (QMS). To prevent absorption bands of CO, CO_2 and H_2O gas in the atmosphere, the IR beam path was built inside vacuum, pumped by dry pump. The main chamber and the IR path are separated by ZnSe windows, which can allow infra-red penetration from 0.5 – 20 um with absorption less than 0.07 %. In this study, the infrared spectra are obtained with resolution of 4 cm^{-1} and averaged over 32 scans. The angle between the IR beam path and the substrate holder is 45 degrees. The QMS (MKS Microvision 2) consists of a controller and mechanical part sealed by a mounting flange in ultrahigh vacuum. It is mounted 10 cm from the substrate and run with a resolution 0.5 a.m.u. The Ionizer release 70 eV electron by filament and ionize incoming molecules to positive charged ions between anode grid and repeller. The ions were accelerated by focus plate and enters ion filter, which consists of four circular rods, with a combination of A.C and D.C. potential to sieve whole bandpass ions at millisecond timescale. The selected ions enter ion detector and are detected by either faraday cup and continuous dynode electron multiplier (CDEM) which can secondary multiply weak signals.

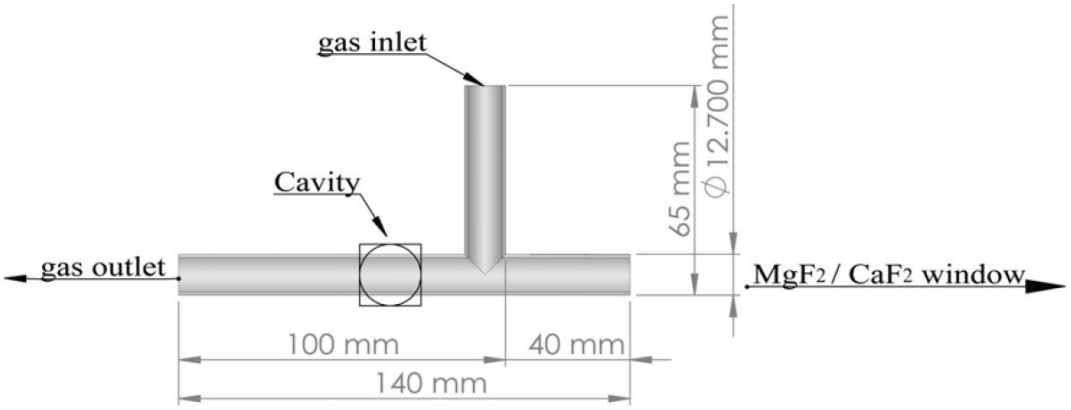

Figure 2.2: The cross-section of MDHL (T-type geometry) (Quoted from Chen et al. 2014).

The samples are prepared in situ in our gasline system. It contains four stainless steel bottles with the same volume, which is used to determine relative proportion of the gas mixtures by their partial pressures. The ammonia gas 99.99 % and methane 99.999 % are mixed with partial pressure measured by a Baratron with 0 - 100 torr range with a 0.25

2.1.2 Vacuum-UV source

In order to simulate the photoprocessing of vacuum ultraviolet (VUV) irradiation onto the interstellar ices and ices on planetary bodies, including KBOs, the ice mixtures are irradiated with a T-type Microwave-Discharged Hydrogen-flow lamp (MDHL). The molecular hydrogen with pressure 0.4 torr flows through the lamp with a support of a mechanical pump. Using a 2.4 GHz microwave generator and high voltage discharge, a low pressure plasma is produced in the Evenson cavity. Figure 2.2 shows a cross-section of T-type quartz tube; the middle part of the T-type quartz tube is being tunned by a ceramic rod that is called Evenson cavity. In order to measure the photon flux in situ, we use an 88 % transmittance nickel mesh with its photoelectric efficiency being obtained by high-flux beamline in National Synchrotron and a SXUV 100 photodiode calibrated by NIST. A MgF_2 window is placed between the lamp and the sample holder to prevent penetration of VUV photons with wavelength shorter than 114nm, leads to a cut off at 114nm. Figure 2.3 shows a VUV emission spectrum of a MDHL. It consists in Ly-α (121.6nm) and H_2 molecular emission in 110-180 nm

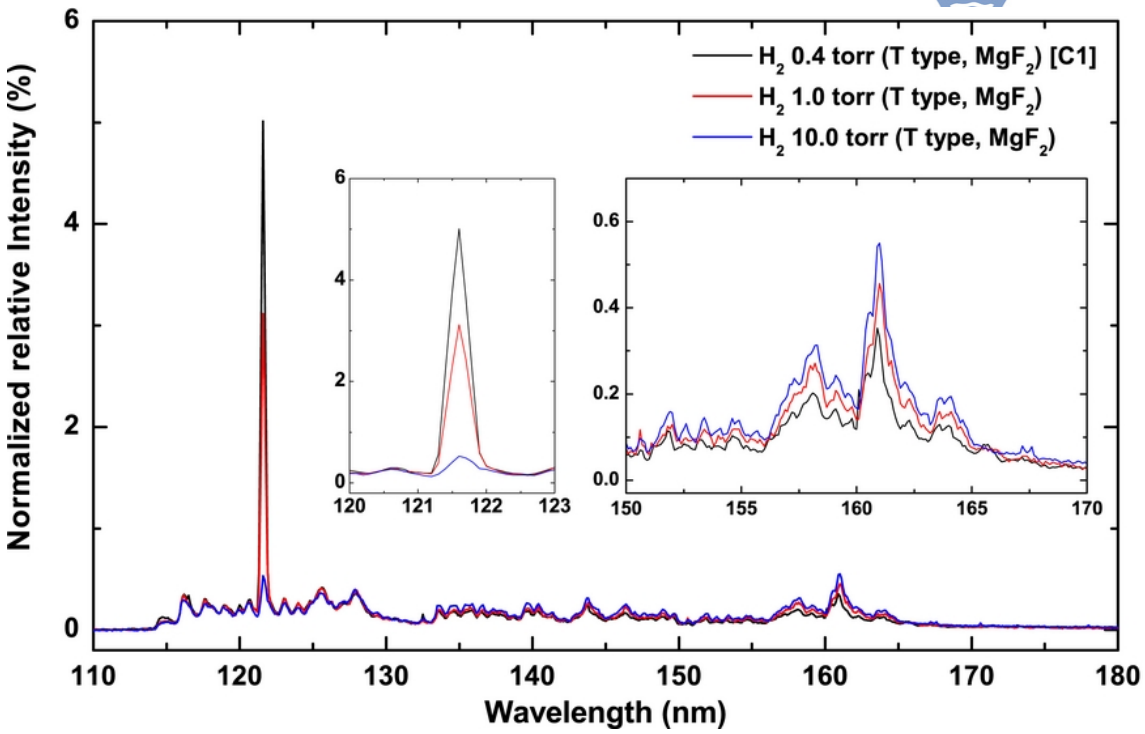

Figure 2.3: VUV spectra of MDHL (T-type geometry, 110-180 nm) with different H_2 pressure inside the lamp(Quoted from Chen et al. 2014).

range. Chen et al. (2014) showed that the spectral characteristics of the VUV light emitted in this range depends on the gas type (mixture of H_2 with He or Ar etc), pressure of H_2 and lamp geometry. Throughout those configurations stated there, we adopted 0.4 torr molecular hydrogen and T-type MDHL that produces VUV irradiation at 114-170 nm with 19.1 % of Ly-α and a mean photon energy of 9.27 eV. The photon flux is 6.4×10^{13} photons $cm^{-2}s^{-1}$ at sample position.

2.1.3 Extreme EUV source

To simulate the solar EUV irradiation reflected by IPM on both Charon and interstellar ices, we use the HF-CGM high – flux beam line of the National Synchrotron Radiation Research Center in Hsinchu, Taiwan. It provides a continuum EUV to VUV photons from 4 to 40 eV. The continuum is separated into monochromatic He II line (30.4nm) with a six-meter cylindrical grating monochrometer with an incident angle of 70 degrees. With the help of a movable entrance slit and movable curved exit slit, the energy resolving power can reach around 3×10^4 at 40 eV for grating 1600 l/mm with both slits movable and set opening to

10 μm (Hsieh 1998). Similar to VUV irradiation provided by MDHL, the light intensity was monitored by the same nickel mesh with photoelectric efficiency obtained by SXUV 100 photodiode calibrated by NIST. With the known photoelectric efficiency, the flux of monochromatic 30.4nm is measured to be 2.15×10^{14} photons $s^{-1}cm^{-2}$ with a spot size of 1 cm

2.2 Experimental Protocol

In this section, we will briefly introduce the procedures of how we performed our experiments. It is divided into four parts, preparation and cooling, deposition, irradiation and warmup.

Preparation of experiments and cooling

Before any of experiment is done, we bake our system at 100 oC for 48 hours to reduce the contamination of water and residue gases as much as possible. It was cooled to room temperature that the background pressure can reach routinely at 1×10^{-10} torr. The gasline were connected with the regulators of the gas tanks and bake to 100 ^oC and pumped by molecularturbo pump for two days before any experiment were done. Also, The water sample has been freeze thaw several times by liquid nitrogen until there is no pressure increase recorded by baratron when water is freezed. Before cooling the substrate to cryogenic temperature, we took an IR spectrum and started the monitoring of residue gases by QMS in order to compare the residue molecules and to verify any possible contaminations in the main chamber. We then start the cooling process thanks to the closed-cycle He cryostat.

Deposition

The gas mixtures are pre-mixed in our gasline system introduced in section 2.1.1. We used a leak valve to condense the gas from the stainless steel bottles onto pre-cooled KBr substrate at 14 K, which monitored by Fourier transformed Infra-red spectroscopy (FTIR) and Quadrupole mass spectrometer (QMS) during deposition. The pressure of deposition is fixed to 1×10^{-8} torr that the deposition rate is $4 \times 10^{16} molecules cm^{-2} min^{-1}$. After deposition, we placed the ice mixture at 14 K for 60 minutes and to allow pumping of residue gas, until

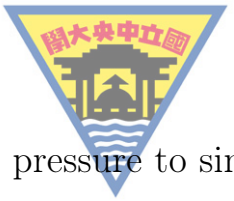

pressure of the main chamber reduce back to its base pressure to simulate the interstellar environment before irradiation.

Photon Irradiation

The total irradiation time is 270 to 450 minutes depend on experiment configurations; with time intervals varies from 2 to 30 minutes. After each irradiation, we waited for 10 minutes allowing pumping out of the photodesorpted gas molecules. During irradiation, the photon flux is monitored by a nickel mesh. After Irradiation, we place the sample for 30 minutes to observe if any thermal reaction was conducted.

Warmup

We use 1 K/min to warmup the substrate to 300 K to demonstrate effects of a new born star nearby an interstellar cloud. During warmup, we record the QMS from 1 to 100 a.m.u. to observe if there are low quantity of higher mass product formed during irradiation.

2.3 Infra-red spectroscopy and the Beer's Law

We used infra-red spectroscopy extensively in chapter 3 and 4, it is a powerful tool in studying molecular interactions during irradiation and warmup. We choose infra-red rather than Ramen spectroscopy because infra-red has lower energy that it would not change the structure of the ice mixture nor breaking any of the bonds. With different vibration modes, the energy absorbed by molecules are quantized. With the energy of absorption bands in infra-red spectrum, we may identify the functional group of the species. To simply classify, molecules can have, from less energetic, translational, rotational and vibrational motions. Generally, vibrational motions can be divided into stretching and bending. Stretching needs more energy than bending. For stretching, there exist Symmetric and Asymmetric stretching, while bending can be divided into In-plane Scissoring, rocking and out of plane Wagging and Twisting (Figure 2.4).

By Beer's Law, we may calculate the column density of the molecule

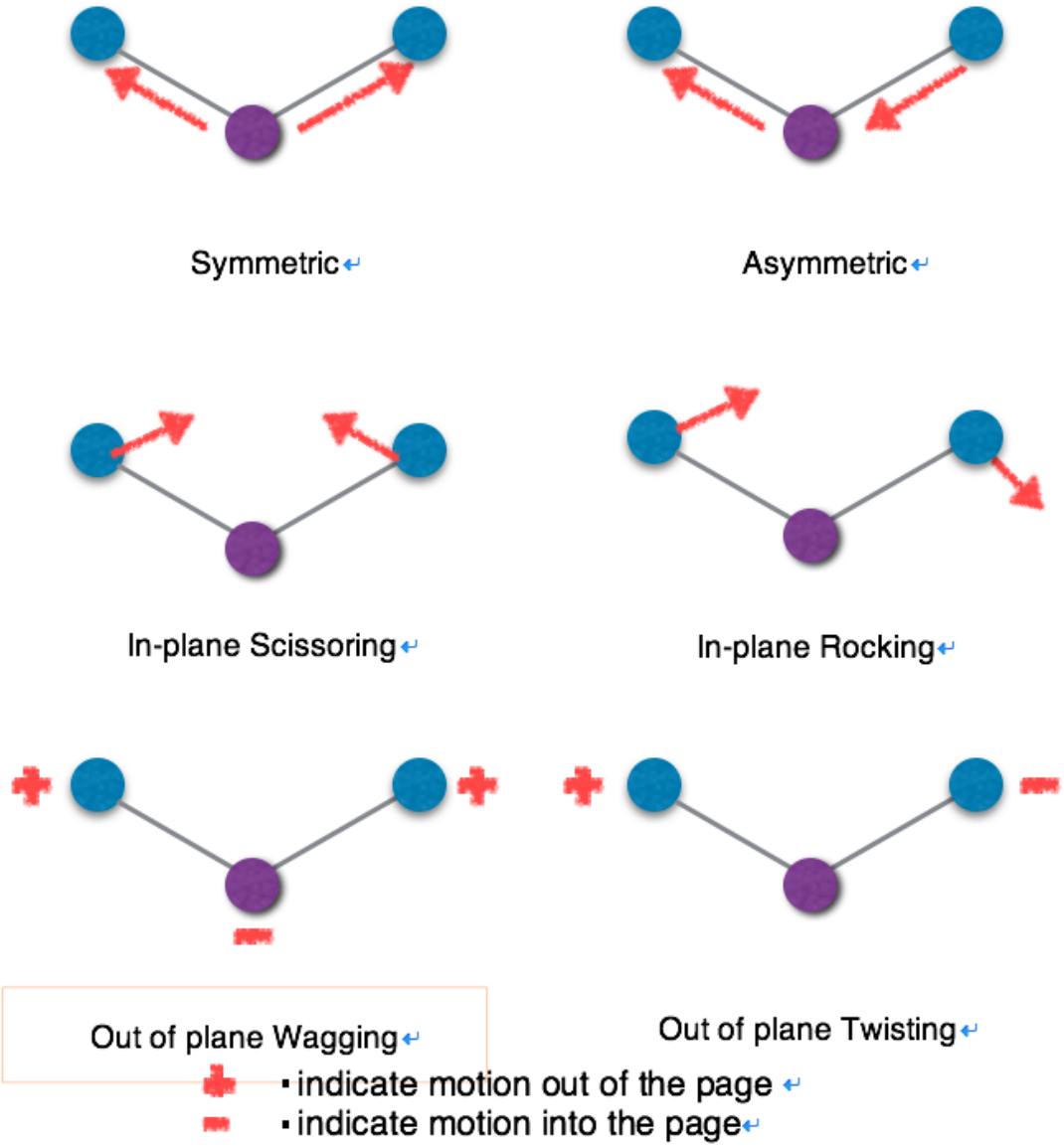

Figure 2.4: Different vibrational modes of a three atom molecule.

with its functional groups, which are used to plot figures in chapter 3 and 4. Beer Lambert's Law suggest that when light passes through a medium, amount of light absorbed is proportional to density and path length of the medium. Assume the known intensity beam $I_0(\nu)$ passes through the medium and beam intensity become $I(\nu)$. The transmittance $T(\nu)$ is defined by equation 2.1.

$$T(\nu) = \frac{I(\nu)}{I_0(\nu)} \tag{2.1}$$

Also, the absorbance $a(\nu)$ is defined by equation 2.2.

$$a(\nu) = -\ln T(\nu) = -\ln \frac{I(\nu)}{I_0(\nu)} = nl\sigma(\nu) \tag{2.2}$$

where n is number density (molecules/cm^3), l is the path length (cm), $\sigma(\nu)$ is the cross-section (cm^2/molecule) of corresponding frequency ν. This equation is known as Lambert Beer's Law.

As the ice mixture in our thesis are at 14K, the peaks of absorbance are often a broadband due to coupling between neighbor molecules. Therefore, we can integrate the whole band of the peak equation 2.2 with respect to frequency and use the absorbance strength (A value) in literatures to calculate the column densities N of the ices by equation 2.3.

$$N = \frac{\int a(\nu)\mathrm{d}\nu}{A(\nu)} \tag{2.3}$$

where N is the column density (molecule cm^{-2}), $A(\nu)$ is the absorbance strength (cm molecule^{-1}).

2.4 Reaction Rate Laws

In this section, we will introduce rate reaction of a consecutive reaction and the concept of pseudo first order which we used to fit our reaction product against irradiation time. The rate of a chemical reaction is the relation between change in concentration of a substance per unit of time. i.e. For a balanced chemical reaction, A $\rightarrow$ 2B, the rate of

reaction is $-\frac{\Delta[A]}{\Delta t}$. The formation rate of B is 2 times destruction rate of A.

When there are two reactants, with balanced equation 2A + B $\rightarrow$ 2C. The reaction is a third order overall, second order in A and first order in B. rate $= k[A]^2[B]$.

To determine the order of a reaction, we can only determine it experimentally. One way is method of initial rates. By changing concentration of initial reactants, and find out the initial reaction rate, we may find out the relation between two reactants and the rate. i.e. rate $= k[A]^x[B]^y$. For a reaction with only one reactant $[R]$, we may use the relation between time and reactant concentration to plot graphs to find out the order or reaction. For a zero order reaction, the rate is not depending on any reactant that it is a constant. The rate $= -\frac{\Delta[R]}{\Delta t} = k[R]^0$. By calculus, $[R]_0 - [R]_t = kt$.

For a first order reaction, rate $= -\frac{\Delta[R]}{\Delta t} = k[R]$. By calculus, $\ln[R]_t = -kt + \ln[R]_0$.

For a second order reaction, rate $= -\frac{\Delta[R]}{\Delta t} = k[R]^2$. By calculus, $\frac{1}{[R]_t} - \frac{1}{[R]_0} = kt$.

Hence, if we get a straight line in a plot between time as x-axis, and the concentration of reactant as y axis, it is a zeroth order reaction, similarly, in first order reactions, we get straight line in plots between $\ln[R]$ as y axis and t in x axis.

In a reaction with one reactant in excess, the rate of reaction is called pseudo first order reaction where pseudo means pretended. For A+B $\rightarrow$ C, rate $= k[A][B]$. As $[B]_0 \gg [A]_0$, change of $[B]$ is negligible that $[B] \sim [B]_0$. Therefore, $[B]$ is assumed to be a constant and included in the rate constant k.

For a consecutive reaction, where A $\rightarrow$ B $\rightarrow$ C that the produced product will not convert back as reactant. A simple example is radioactive decay. At $t = 0$, $[A] = [A]_0$, $[B] = 0$, $[C] = 0$ and at all times, $[A] + [B] + [C] = [A]_0$. The rate equations are as follows:

$$-\frac{\Delta[A]}{\Delta t} = k_1[A] \tag{2.4}$$

$$-\frac{\Delta[B]}{\Delta t} = k_1[A] - k_2[B] \tag{2.5}$$

$$-\frac{\Delta[C]}{\Delta t} = k_2[B] \tag{2.6}$$

By equation 2.4, we get

$$[A] = [A]_0 e^{-k_1 t} \tag{2.7}$$

By substituting equation 2.7 into equation 2.5, we get

$$-\frac{\Delta[B]}{\Delta t} + k_2[B] = k_1[A]_0 e^{-k_1 t} \tag{2.8}$$

After solving the differential equation 2.8 , we get

$$[B] = \frac{k_1}{k_2 - k_1}(e^{-k_1 t} - e^{-k_2 t})[A]_0 \tag{2.9}$$

Finally, since $[C] = [A]_0 - [B] - [A]$, by equation 2.7 and 2.9, we get

$$[C] = \left(1 + \frac{k_1 e^{-k_2 t} - k_2 e^{-k_1 t}}{k_2 - k_1}\right)[A]_0 \tag{2.10}$$


國立中央大學

3. Results and Discussions

According to Grundy et al. (2016), CH_4 from Pluto may accumulate by cold-trapping, onto surface of Charon. The amount of CH_4 varies throughout the surface of Charon because it depends on duration of temperature below 25 K. The duration depends on diurnal motion and thermal inertia of Charon. With a tilted axis of 112 degrees to the ecliptic, higher concentration of CH_4 will accumulate at the pole (see chapter 1 for details). Therefore, we investigate different concentrations of CH_4+NH_3 ice mixtures and answer several questions: Will different concentration of CH_4 mix with high concentration of ammonia observed on crater position and throughout the surface of Charon (Grundy et al. 2016) have structure difference in accumulation of tholin? Are there variations of photo-products when concentration of CH_4 differ during warm-up? Since both EUV and VUV irradiation irradiates onto Charon, are there any differences when we change the photon source from VUV to EUV to irradiate the ice mixtures?

The main source to irradiate the dark side of Charon is Lyα reflected by interplanetary medium (Grundy 2016). Other sources such as the energetic ions in solar wind, consists of mainly H^+, He^+, He^{++} and O^{2+} etc are originated from solar corona or IPM. These ions would also reflect solar irradiation to the dark side of Charon. Among these irradiations, we picked He II irradiation because He II is 3 – 20 times more intense then He I during a solar flare. As it varies, it is difficult to estimate the dose onto Charon. Besides, electronic flux is also present in solar wind but it is one order of magnitude lower than proton flux. The flux for energetic electrons observed at the 1 A. U. position is available (http://www.swpc.noaa.gov/products/goes-electron-flux). Although electron flux is much less important than Lyα, and their flux

varies, we also compare the electron irradiation experiment done by Kim and Kaiser (2011) on CH_4+NH_3 ice mixtures in this chapter.

When Charon is shine by direct sun light, the surface temperature increases and deliver the heat to the poles by conduction. From the model of Grundy et al. (2016), the surface temperature of the pole area would increase to 60 K that the heating rate depends on the thermal conductivity of Charon. To demonstrate the heating process, we warmup our ice mixture with a heating rate 1 K/min and monitor the ice by both QMS and scanning IR spectra with 5 K intervals. We will look into whether there are new species formed during warmup and monitor the gas phase desorption.

Finally, in this chapter, after we focus on the concentration effect of CH_4 on photo-products, photon energy effects, species detected during warmup phases, we present the residues accumulated by irradiating CH_4+NH_3 ice mixtures with different ratios. Since both tholin formed on Titan and Charon has similar colour, we also compare the IR spectra of MDHL, NSRRC with different configurations with the residues on Titan with experiments done by Imanaka et al.

3.1 The infra-red spectrums and peaks identification

Before and after deposition, we scanned an IR spectrum and plotted the absorbance of the ice mixtures. Figure 3.1 is a plot of the absorbance of the CH_4+NH_3 ice mixtures in different ratios of CH_4+NH_3 ice mixtures, from top to bottom 1:20, 1:10, 1:5 and 3:2. We have labelled the peaks which we used to calculate the column densitiesby dotted lines throughout the graph. Main products we have detected are C_2H_6, CN^- and C_3H_8. The peak positions with the references are listed in Table 3.1.

We integrated the area and divided by the absorption strength stated in table 3.2. Although we understand that there is an average error in absorption strengths of no more than 10 % when the pure ice is diluted in N_2 and H_2O (Richey and Gerakines 2012). In our case,

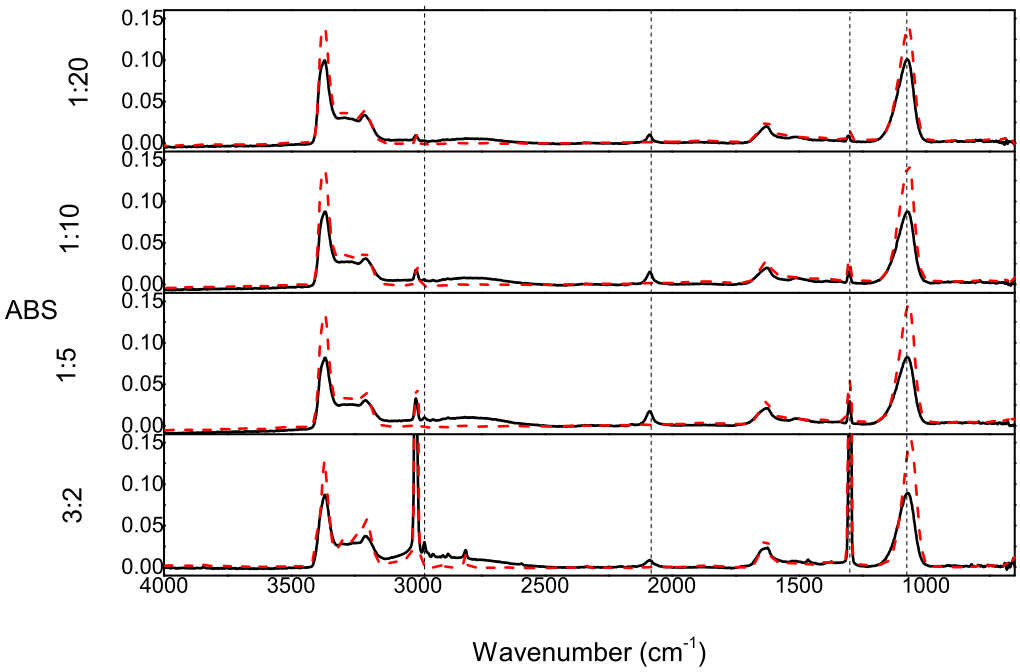

Figure 3.1: The the infra-red spectrum of CH_4 + NH_3 ice mixtures before irradiation (dashed) and VUV irradiated ice mixtures provided by MDHL.

Table 3.1: The peak positions of identified substances after irradiation in different configurations of ice mixtures.

Literture assignments		CH_4+NH_3 ratio (MDHL)				
Wavenumber (cm^{-1})	Carrier	1:5 (cm^{-1})	1:10 (cm^{-1})	1:20 (cm^{-1})	3:2 (cm^{-1})	Ref.
3375	ν_3 (NH_3)	3366	3366	3369	3367	1
3290	$2\nu_4$ (NH_3)	-	-	-	-	1
3210	ν_1 (NH_3)	3207	3208	3210	3205	1
3011	ν_3 (CH_4)	-	-	-	-	2
2972	ν_{10} (C_2H_6)	2975	-	-	2975	3
2960	C_3H_8	-	-	-	2960	7
2941	$\nu_8 + \nu_1 1$ (C_2H_6)	2940	-	-	2940	3
2904	ν_1 (CH_4)	2901	-	-	2901	5
2879	ν_5 (C_2H_6)	2882	2883	-	2882	3
2814	$\nu_2 + \nu_4$ (CH_4)	-	-	-	2815	5
2083	ν (CN^-)	2088	2087	2088	2088	2
1625	ν_4 (NH_3)	1625	1625	1626	1631	1
1514	δ (NH_2)	1509	1507	1505	1511	6
1465-1440	deform CH_2 scissor	1461	-	-	1463	3,4
1390-1370	CH_3 sym deform	1394	1394	1394	1372	4
1298	ν_4 (CH_4)	1301	1302	1305	1299	2
1075	ν_2 (NH_3)	1073	1072	1072	1072	1
820	$\nu_1 2$ (C_2H_6)	-	-	-	820	3

Reference: 1. Bossa et al 2008 2. Moore and Hudson 2003 3. Kim et al. 2010 4. Socrates 2001 5. Bennet and Kaiser 2007 6. Zheng et al. 2008 7. Hudson and Moore 2004

absorption strengths changes after CH_4 and NH_3 are mixed. For example, according to d' Hendecourt and Allamandola (1986), the band of NH_3 located at 1070 cm^{-1} would not change much (from 1.1×10^{-17} to 1.2×10^{-17}) when excess water is added to pure NH_3 and therefore, we may use the same absorption strength throughout our discussion to give a brief concept on what is the column density of the species and how is the absorption area changes when concentrations of ice mixtures and photon energy are changed. For the case of CN^-, we know that CN^- has a bond order =3 by its molecular orbitals which is different from CN stretching (bond order 2.5) which is very sensitive to the matrix environment. As an example, by Borget et al. (2012), the CN stretch in amino acetonitrile change by factor of 2 between the pure molecule itself and in a mixture of amino acetonitrile and H_2O (1:3). Here, we adopt the absorption strengths stated in Table 3.2 and neglect the error in absorption strengths.

Table 3.2: The strength of absorbance adopted in this thesis measured in literatures of pure ice samples

Wavenumber (cm^{-1})	Assignment	Vibration	FWHM	A value ($\times 10^{-17}$)	Reference
2976	C_2H_6	$-CH_3$	-	1.05	2
2960	C_3H_8	$-CH_2-$	-	2.58	2
2086	CN^-	CN	-	1.8	3
1297	CH_4	CH deformation	8	0.61	1
1070	NH_3	"umbrella mode"	68	1.7	1

Reference: 1. d'Hendecourt and Allamandola (1986) 2. Moore and Hudson (1998) 3. Noble et al. (2013)

3.2 Reaction mechanisms

3.2.1 C_2H_6

The assignment of C_2H_6 is confirmed by several bands listed in table 3.1. Figure 3.2 is a partial of figure 3.1. The absorption peak located at 2075 cm^{-1} is the strongest vibration of C_2H_6. The formation mechanism of C_2H_6 in astrophysical environment is proposed by Bennet et al. (2006), that the main route to form C_2H_6 is by a combination of 2 CH_3 radicals (equation 3.1 and 3.2):

$$CH_4 + h\nu \rightarrow CH_3 \tag{3.1}$$

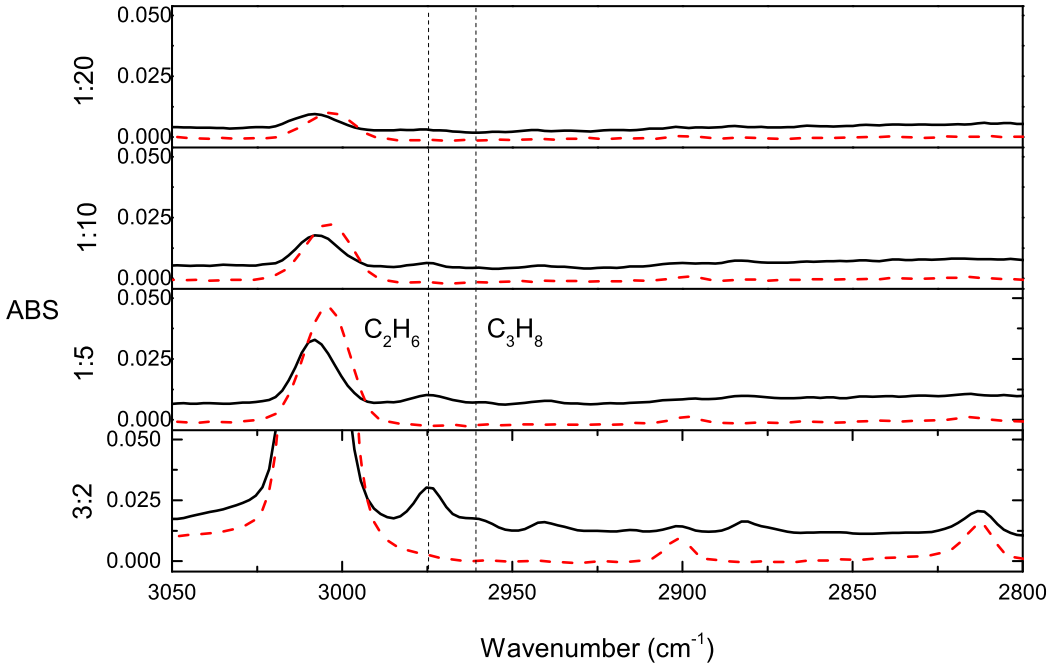

Figure 3.2: The the infra-red spectrum of CH_4 + NH_3 ice mixtures of C_2H_6 and C_3H_8 before irradiation (dashed) and VUV irradiated ice mixtures provided by MDHL.

$$2CH_3 \rightarrow C_2H_6 \tag{3.2}$$

The energy required to produce 1 CH_3 radical from CH4 is 4.42 eV. 2 CH_3 radicals recombine to form C_2H_6 releases 3.74 eV. Therefore, equation 3.2 is a no-barrier exothermic process. However, C_2H_6 is not detected in CH_4+NH_3=1:20 ice mixtures. Figure 3.3 shows the temporal formation column density of C_2H_6 in different configurations of irradiated ice mixtures. As the formation only depends on CH_4, we may use first order kinetics equation to fit the column density versus photon dose.

$$[A] = [A]_0(1 - e^{-k_1 t}) \tag{3.3}$$

to fit the formation of C_2H_6. The fitting results are shown in table 3.3.

Table 3.3: The fitting results of C_2H_6 by $[C_2H_6]=[C_2H_6](1 - e^{-k_1 t})$

Ratio of CH_4+NH_3	A (x10^{15} molecules cm^{-2})	k (x10^{-17} $photon^{-1}$)
1:10	2.90 ± 1.25	0.92 ± 0.15
1:5	4.16 ± 0.28	2.28 ± 0.28
3:2	19.2 ± 0.15	5.28 ± 0.25

From table 3.3, production rate is also proportional to the initial

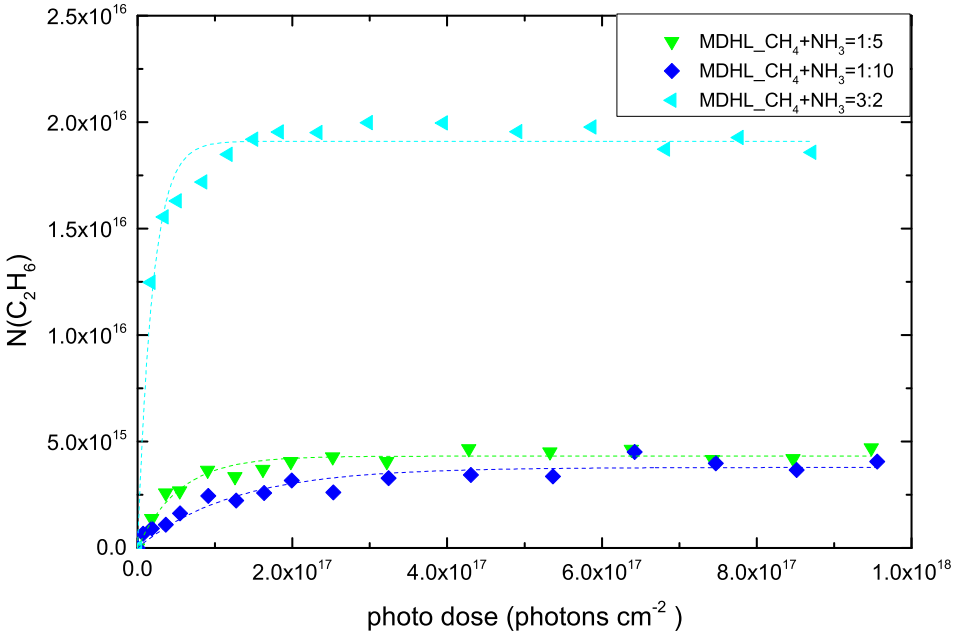

Figure 3.3: The column density of C2H6 during CH4 + NH3 ice mixtures irradiated by MDHL.

CH_4 concentration.

3.2.2 C_3H_8

The peak positioned at 2960 cm^{-1} belongs to –CH_2- so we assigned that as C_3H_8, as the shortest carbon chain. The signal to noise ratio in CH_4+NH_3 = 1:10 is poor that we can not quantize the amount of C_3H_8 (figure 3.2).

It is a secondary product formed by a combination of either C_2H_6 + CH_2 (equation 3.4)or C_2H_4 + CH_4 (equation 3.5).

$$C_2H_6 + CH_2 \rightarrow C_3H_8 \tag{3.4}$$

$$C_2H_4 + CH_4 \rightarrow C_3H_8 \tag{3.5}$$

By modern peak fitting method, we deconvoluted the overlapped C_2H_6 and C_3H_8 into two gaussians.

3.2.3 CN^-

From infra-red absorption spectrum (figure 3.4) and their positions, we assigned the peak 2086 cm^{-1} to CN^- but not a combination of HCN and CN^-. The assignment is based on a absence in CN bending mode at

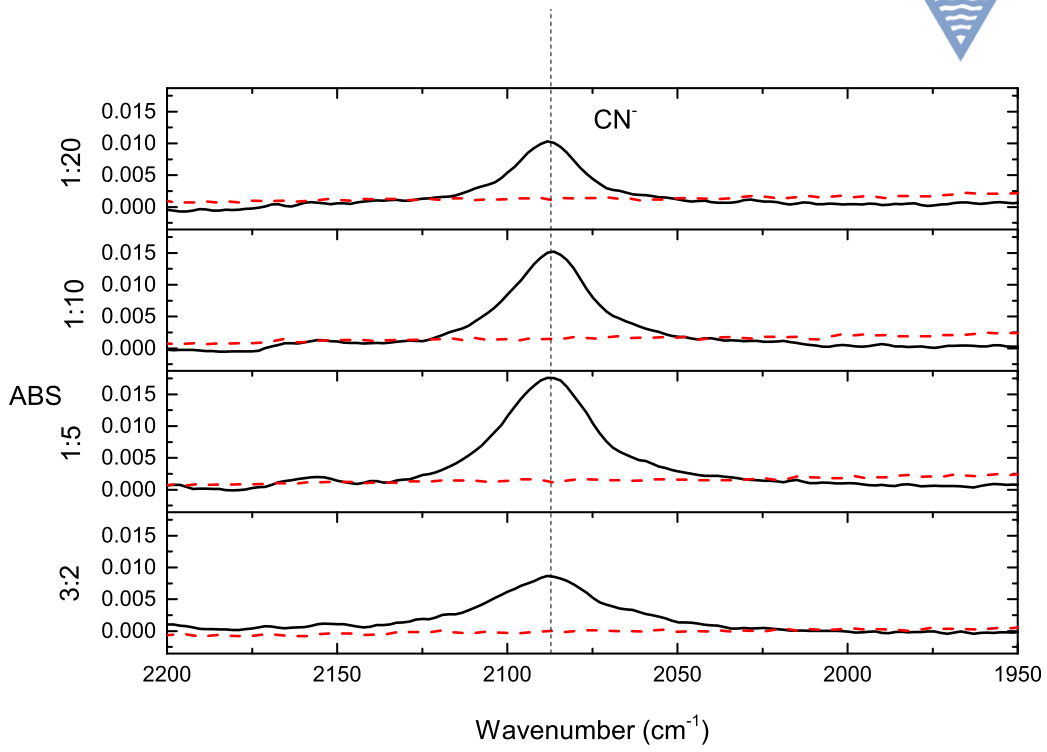

Figure 3.4: The the infra-red spectrum of CH_4 + NH_3 ice mixtures of C_2H_6 and C_3H_8 before irradiation (dashed) and VUV irradiated ice mixtures provided by MDHL.

848 cm^{-1}. In the case CH_4 + NH_3 = 3:2, we may observe a peak located at 820 cm^{-1}, which is with a FWHM half of HCN and it is eliminated at 50 K during the warm-up phase. Since 50 K is the desorbing temperature of C_2H_6 and the peak position is the close to v12 mode of C_2H_6, we believe that the 820 cm^{-1} peak is contributed by C_2H_6. Therefore, we may assign our peak located at 2086 cm^{-1} as purely CN^-.

The formation mechanism of CN^- at low temperature was first suggested by Kim and Kaiser (2011) to be two step reaction mechanism with methylamine as intermediate. CH_4 and NH_3 irradiated by photon to become CH_3 and NH_2 radical (figure **??**, followed by propagation and recombination of radicals becoming CH_3NH_2 and dehydrogenation and acid-base reaction to form CN^-. Although Kim and Kaiser used 1.5keV electron as energy source to simulate the cosmic ray induced photochemistry, this formation mechanism also applies in our photon irradiation experiments because we can also detect the methylamine

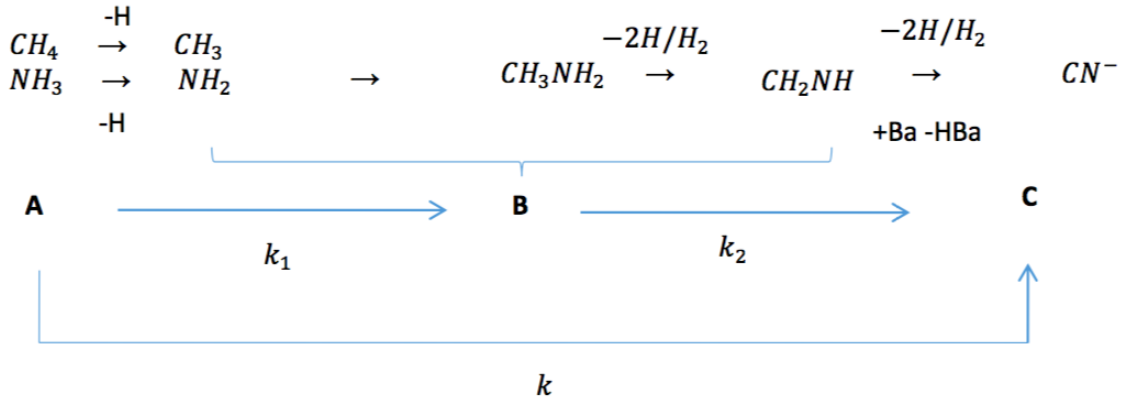

Figure 3.5: The formation mechanism of CN^- proposed by Kim and Kaiser(2011).

during our warm-up phase. The ion fragment with m/z=31 is assigned as $CH_3NH_2^+$ and detectable in all ratios of our CH_4+NH_3 experiments (figure **??**).

By the deviation performed in section 2.4, we have a rate equation for consecutive reactions 2.10. With one of the reactant larger than another, we applied the pseudo first order assumption. With equation 2.10, we fitted the formation of CN^- (figure 3.7)and found that one of the rate constant is always larger than the other in all of the ratios. The fitting results are averaged by more than two experiments and are shown in table 3.6.The results of Kim and Kaiser is also listed into the table, they could observe a two-step reaction mechanism in production of CN^- in CH4+NH3 (3:1) experiments with electron current 0.1 μA. However, when they increased the electron flux to 1 μA for irradiation $C_nH_{2n+2(n=1-6)}$ and NH_3 ice mixtures, they also observed a one-step reaction mechanism.

Table 3.4: The fitting results of CN^- by equation 2.10

Ratio of CH_4+NH_3	A (x10^{16} molecules cm^{-2})	k_1 (x10^{-18} photon^{-1})	k_2 (photon^{-1})
1:20	4.75 ± 0.40	0.70 ± 0.09	>1
1:10	4.51 ± 0.18	1.33 ± 0.13	>1
1:5	4.61 ± 0.18	1.93 ± 0.19	>1
3:2	2.24 ± 0.03	8.21 ± 0.70	>1

A represents the amount of CN^- we may obtain when irradiated the ice for infinitely long.

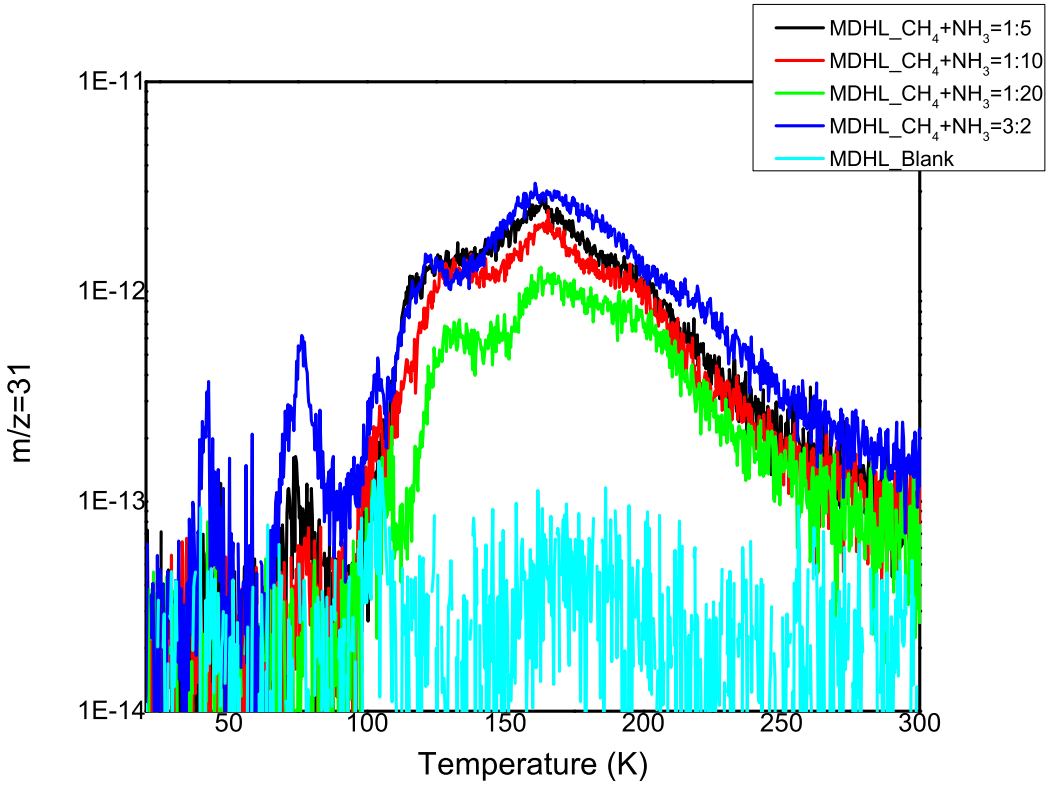

Figure 3.6: The m/z=31 detected by QMS during warm-up with heating rate 1 K/min in different configurations of ice mixtures.

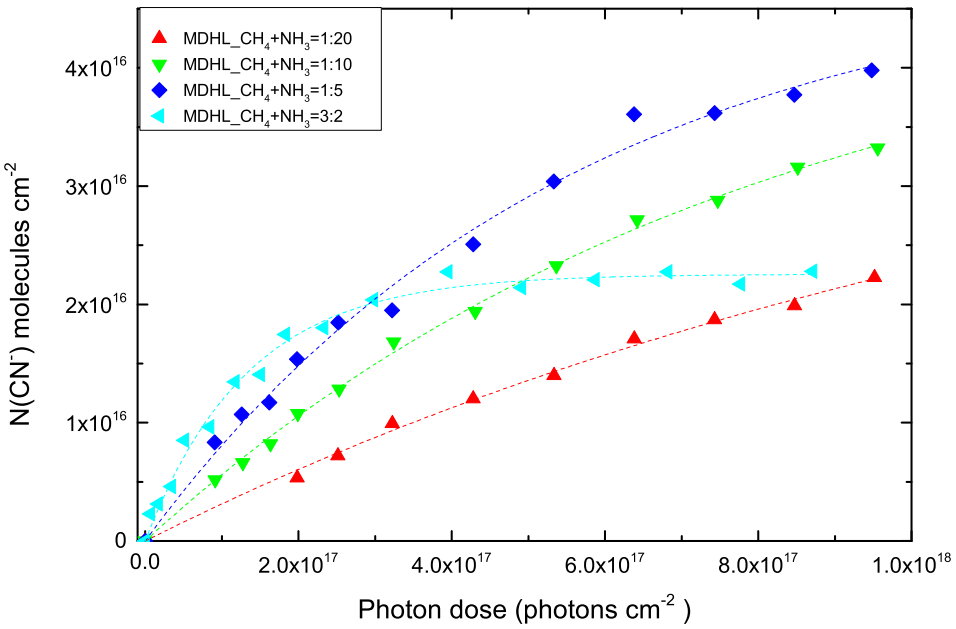

Figure 3.7: The column density of CN^- accumulated when different configurations of CH_4 + NH_3 ice mixtures are irradiated by VUV photons provided by MDHL. The dotted lines are fits of column densities by equation 2.10.

3.3 The Concentration Effect in formation of Cyanide ions and Ethane

3.3.1 Cyanide ion

From table 3.6, we may see that the rate k_1 is proportional to the concentration of CH_4. The rate constant k_1 increases when concentration of CH_4 increases. Since NH_3 is fixed in all of our experiments, more CH_4 are evolved into CH_3 radical formation when proportion of CH_4 in the ice mixture increases. More abundant CH_3 radicals in the ice mixtures would produce more CH_3NH_2 intermediates.

In CH_4+NH_3 =3:2 ice mixtures, A is half of the other ratios. The reduction is mainly because CN^- has a competing relationship with formation of C_2H_6 and C_3H_8. NH_2 radicals competes with CH_2, CH_3 and C_2H_4 radicals. With this competition, the intermediate CH_3NH_2 is reduced. Therefore, in ratio 3:2 CH_4+NH_3 ice mixture, the yield of CN^- is the least(table 3.6). Note that the formation yield of C2H6 is the maximum in this ratio (table 3.3)

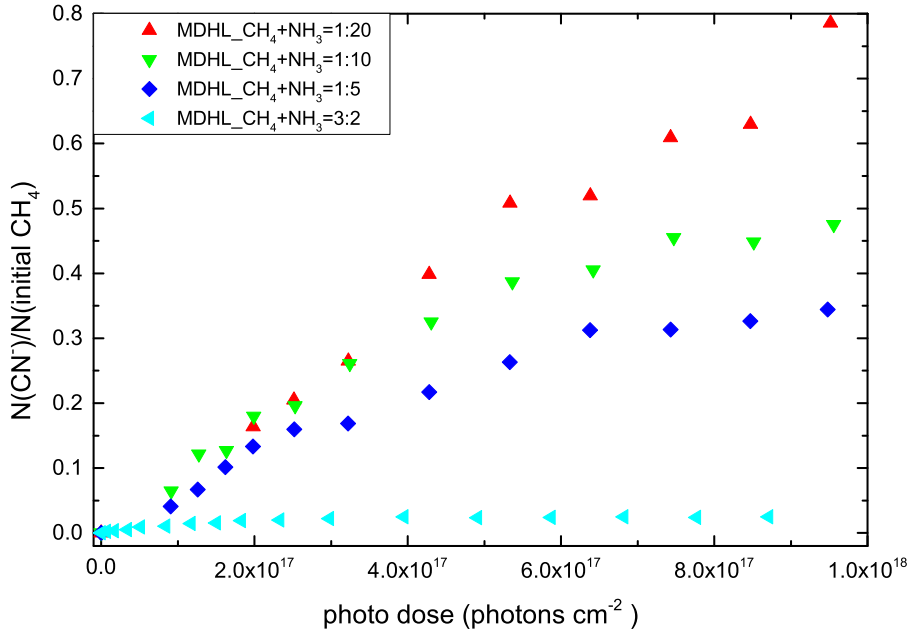

Figure 3.8: The column density of CN^- divided by initial CH_4 accumulated when different configurations of CH_4 + NH_3 ice mixtures are irradiated by VUV photons provided by MDHL.

Considering the normalized CN^- with respect to the initial CH_4(figure 3.8), the formation of CN^- is more effective in low CH_4 concentration ice mixtures. The mobile CH_3 radical is aggregated by excess NH_3. In this situation, CH_3 radicals have less chance to meet another CH_3 radical or C_2H_4. It is more likely to react with NH_2 radicals so the formation of CN^- in low CH_4 concentration ice mixtures are more efficient.

3.3.2 Ethane

Considering the case of ratio of CN^- divided by C_2H_6,the formation of CN^- in ice mixtures with diluted CH_4 has more CN^- formed then C_2H_6. It is because ice mixtures with with higher concentrations in CH_4 is more effective for one CH_3 radical to combine with another CH_3 radical. On the contrast, CH_3 radicals formed in the ice mixtures with diluted CH_4 concentrations are aggregated by NH_3. Therefore, CN^- is less efficient to form in ice mixtures with excess NH_3.

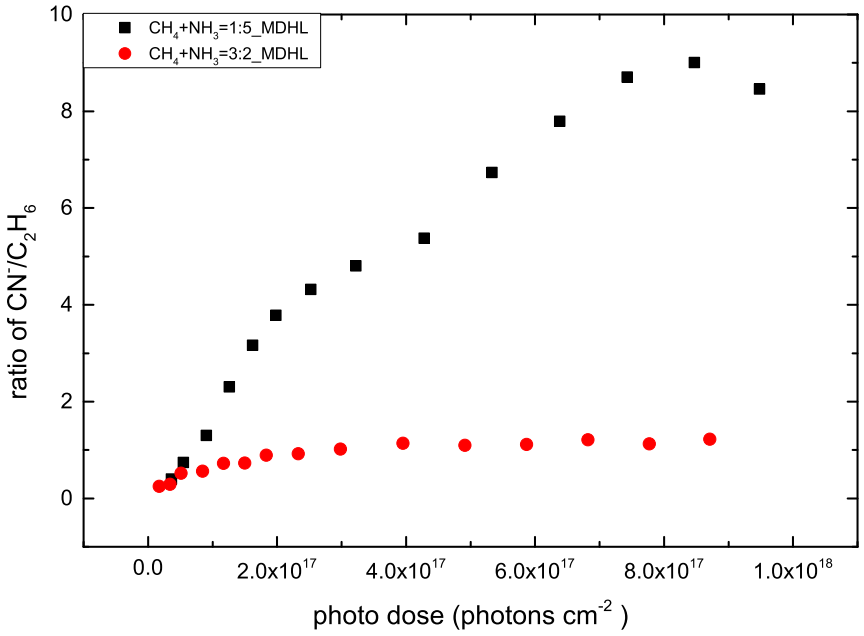

Figure 3.9: The column density of CN^- divided by C_2H_6 accumulated when different configurations of CH_4 + NH_3 ice mixtures are irradiated by VUV photons provided by MDHL.

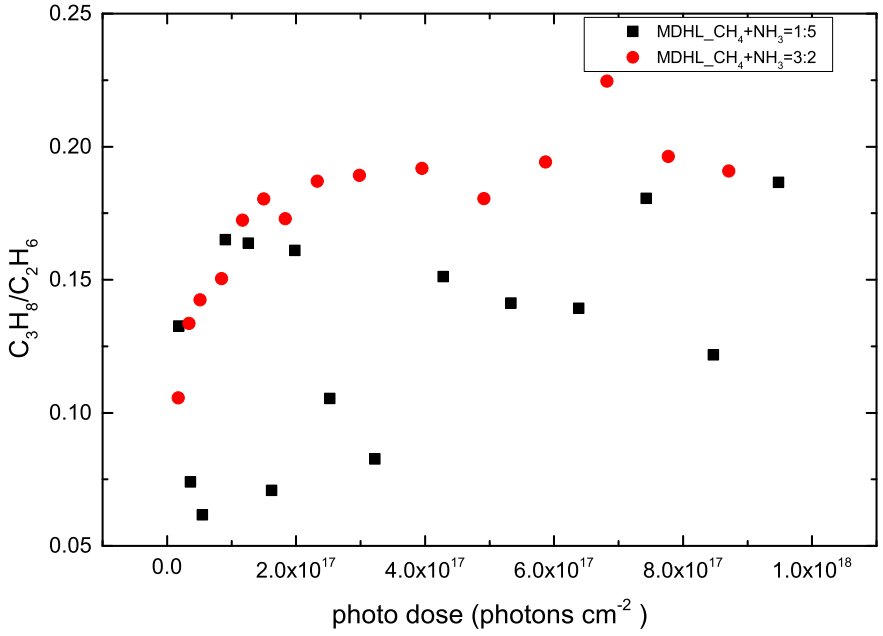

Figure 3.10: The column density of C_3H_8 divided by C_2H_6 accumulated when different configurations of CH_4 + NH_3 ice mixtures are irradiated by VUV photons provided by MDHL.

3.3.3 Propane

C_3H_8 forms based on to the C_2H_6 3.10 is the plot with column densities of C_2H_6 divided by C_3H_8. We may see that the ratio in CH_4+NH_3 =1:5 experiment is around 6 where CH_4+NH_3 =3:2 is around 3. This shows that the amount of C_3H_8 in CH_4+NH_3 =3:2 experiment is higher. It is rather difficult for C_3H_8 to form in CH_4+NH_3 = 1:5 experiments because NH_3 aggregated them. The formation of C_3H_8 in CH4+NH3 =1:5 and 3:2 experiments has given a reasonable explanation about why C_2H_6 formation is most efficient in CH_4+NH_3 =1:10 experiments.

3.4 Cyanide ion produced by photon source and electron source

We study the ice mixtures of CH_3 dominated ice mixtures and compare the efficencies in CN

We calculated the percentage of photons absorbed by CH_4+NH_3 ice mixtures in different configurations. Applying cross-sections measured by Cruz-Diaz et al. (2014) and the spectrum of our MDHL and substitute them into Beer's law. In CH_4+NH_3 = 3:2 ice mixtures with ammonia fixed at 600 ML can absorb more than 99.9 % of light. Therefore, we may assume all the irradiated light is absorbed by the ice. For CH_4+NH_3 =3:2 ice mixture, around 9×10^{17} photons were irradiated in 270 minutes.

In Kim and Kaiser (2011) electron irradiation experiments, the energy transferred to CH_4 + NH_3 ice mixtures is by linear electron transfer (LET) that 1.3 eV molecule^{-1} was absorbed by the ice in 90 minutes. They get flattened at 20 minutes' irradiation, with fluence of 2.0×10^{14} electrons cm^{-2}. While we got flattened at a dose of 3×10^{17} photons cm^{-2}. Considering the energy of their electron (1.5 keV) and energy of our photons, they got flattened at 3×10^{17} eV cm^{-2} while we get flattened at 27.81×10^{17} eV cm^{-2}. Comparing these energy doses, less electrons are needed to flatten the formation of CN^-.

Comparing our CN^- obtained after infinitely long exposure, 13 – 16 ML of CN^- was obtained by electron irradiation depending on which equation they choose to fit. In our MDHL experiments, we have 14.8 ML

of CN^-. However, Kim and Kaiser (2011) adopted the CN^- absorption coefficient measured by Georgieva and Velcheva (2006) to be 3.7 x 10^{-18} cm $molecule^{-1}$, which is 4.86 times smaller. We do not adopt this absorption coefficient because it violates the carbon balance that number of CN^- produced will be larger than CH_4 consumption. If we adopted the same absorption coefficient, the production yield of CN^- should be multiplied by 4.86. Therefore, our yield is 72 ML of CN^-. Regarding percentage of NH_3 (limiting reactant), Kim and Kaiser has 5 - 6 % yield where we have 12 % yield if we adopted the same absorption coefficients. To conclude, electron irradiation has a smaller absorption cross-sections, the percentage of yield is also smaller than VUV irradiated ice mixtures with similar ice thicknesses.

3.5 Photon Energy Effect - EUV and VUV

According to Blanksby and Ellison, the dissociation energy for CH_4, becoming CH_3, CH_2 CH and C are 4.55, 4.79, 4.39 and 3.51 eV respectively at 298 K. Whereas dissociation energy for NH_3, becoming NH_2 is 4.67 eV at 298 K.

Considering our MDHL with average energy of 9.27 eV, all of the above fragments may exist rather in the form of radicals or combined with other radicals to form heavier molecules in our ice mixtures. It is not nessesary to further increase the photon energy in order to get another new fragmentation pathway. However, the fragmentation of CH_4 and NH_3 depends on photon energy.

Several gaseous state measurements also presents this result. First, gans et al. (2011) changed photon wavelengthes from 121.6 nm to 118.2 nm to dissociate the CH_4 molecules and ionize the fragments with the corresponding photon energy. Changing from 121.6 to 118.1 nm significantly changed the ionized fragmentation ratio from CH_3^+ and CH_2^+ 1: 1 to 1:2 using pulsed laser. This slightly change of photon energy, from 10.2 eV to 10.4 eV has a significant change in the fragmentation of CH4.

Second, Tsai et al. used 30.4 nm to photo dissociate CH_4 and test it by time – of – flight mass spectrometer yields CH_3^+: CH_2^+: CH^+: C^+ = 1 :0.32: 0.118: 0.0237 (Tsai 1980). Since it is also a gaseous state experimental results, we cannot directly apply this fragmentation into

our calculations. Note that the VUV absorption spectra of CH_4 in solid phases is different from gaseous phases (Cruz-Diaz 2014), so the exact photo dissociation fragmentation ratios by 30.4 nm nor VUV irradiations in astronomical environments are still unknown.

Thirdly, a group also varies ratios of CH_4 + NH_3 mixtures and irradiate with far UV irradiation at 134 nm (Bossard 1980). However, this group only used gas chromatography to analyse the final products and their reaction is carried in gas phase in room temperature. Although the photon energy of our MDHL is enough to dissociate both the CH_4 and NH_3 molecules, we further increase photon energy to He II 30.4 nm to examine whether there are differences in photo-products. It is worthwhile for us to perform experiment by EUV irradiation to see if the EUV irradiation can generate any new products on the surface of Charon, or any difference in yield. After investigation, we may answer several questions: Are there any differences in products or production yields? Would the formation mechanism change?

Table 3.5 shows the identified peaks of CH4+NH3 ice mixtures irradiated by EUV 30.4 nm irradiation provided by NSRRC.

Table 3.5: The peak positions of identified substances after VUV and EUV irradiations in different configurations of ice mixtures.

Literture assignments		CH_4+NH_3 ratio (MDHL)		CH_4+NH_3 ratio (30.4 nm)		
Wavenumber (cm^{-1})	Carrier	1:5 (cm^{-1})	3:2 (cm^{-1})	1:5 (cm^{-1})	3:2 (cm^{-1})	Ref.
3375	ν_3 (NH_3)	3366	3367	3368	3368	1
3290	$2\nu_4$ (NH_3)	-	-	-	-	1
3210	ν_1 (NH_3)	3207	3205	3209	3205	1
3011	ν_3 (CH_4)	-	-	-	-	2
2972	ν_{10} (C_2H_6)	2975	2975 2977	2976		3
2960	C_3H_8	-	2960	-	2960	7
2941	$\nu_8 + \nu_1 1$ (C_2H_6)	2940	2940	-	2942	3
2904	ν_1 (CH_4)	2901	2901	2901	2901	5
2879	ν_5 (C_2H_6)	2882	2882	-	2884	3
2814	$\nu_2 + \nu_4$ (CH_4)	-	2815	-	2813	5
2083	ν (CN^-)	2088	2088	2090	2089	2
1625	ν_4 (NH_3)	1625	1631	1627	1631	1
1514	δ (NH_2)	1509	1511	1509	1511	6
1465-1440	deform CH_2 scissor	1461	1463	-	1465	3,4
1390-1370	CH_3 sym deform	1394	1372	-	1372	4
1298	ν_4 (CH_4)	1301	1299	1303	1301	2
1075	ν_2 (NH_3)	1073	1072	1070	1068	1
820	$\nu_1 2$ (C_2H_6)	-	820	-	-	3

Reference: 1. Bossa et al 2008 2. Moore and Hudson 2003 3. Kim et al. 2010 4. Socrates 2001 5. Bennet and Kaiser 2007 6. Zheng et al. 2008 7. Hudson and Moore 2004

Considering the formation mechanisms of C_2H_6 and C_3H_8, equation (3.2 and 3.4), when changing the photon source from MDHL VUV irradiation to He II 30.4 nm monochromatic light to irradiate CH_4+NH_3 (3:2) ice mixtures, the ratio of C_2H_6 / C_3H_8 of ice mixtures irradiated by VUV irradiation is lower than EUV irradiation provided by NSRRC (figure 3.2.1). There are two probable explanations. First, the fragmentation of CH_4 is different with different photon energies. Therefore, less C_3H_8 is produced with EUV photons. Second, the destruction of CH4 is much less efficient by EUV irradiation. Therefore, the CH_3 radicals are not as rich as the ice mixture irradiated by VUV photons provided by the MDHL. As a result, we further irradiate our ice mixtures by EUV photons until the destruction of CH_4 is similar to VUV irradiation experiments done with MDHL. We found that the second explanation is more persuasive because after CH4 destruction equals to VUV irradiation, the ratio of C_2H_6/C_3H_8 of average of last 7 irradiations is 3.53 and 3.66 in experiments done with 3 experiments with MDHL and 2 experiments in NSRRC respectively. From figure 3.2.2, The reduction of CH_4 is 6.06 times slower in EUV experiments than VUV experiments while the reduction of NH_3 is 3.19$\pm$0.12 times slower. Therefore, the destruction cross-section of CH_4 and NH_3 ice has a 6.06$\pm$0.07 and 3.19$\pm$0.12 times lower in 30.4 nm than in 121.6 nm.

Figure 3.11 shows the column density of C_2H_6 divided by C_3H_8 after CH_4 + NH_3 =3:2 ice mixtures are irradiated by VUV irradiation and He II monochromatic light.

From 3.11, we may observe that more C_3H_8 is produced by 30.4nm photons than by VUV photons. Recall the formation mechanism of C_3H_8 (equation 3.5), CH_2 and C_2H_4 radicals are esccential in producing C_3H_8. This increase production in C_3H_8 may be caused by the increase in CH_2 radicals during fragmentation of CH_4. This result is similar to the findings of Gans et al. (2011), the ratio of CH_2 radicals increases from 0.3 to 0.48 when photon energy increases from 121.6 nm to 118.2 nm in their pulsed laser experiments.

Apart from C_2H_6 and C_3H_8, are there any difference in CN^- production? Figure 3.13 shows the accumulated column densities of CN^-

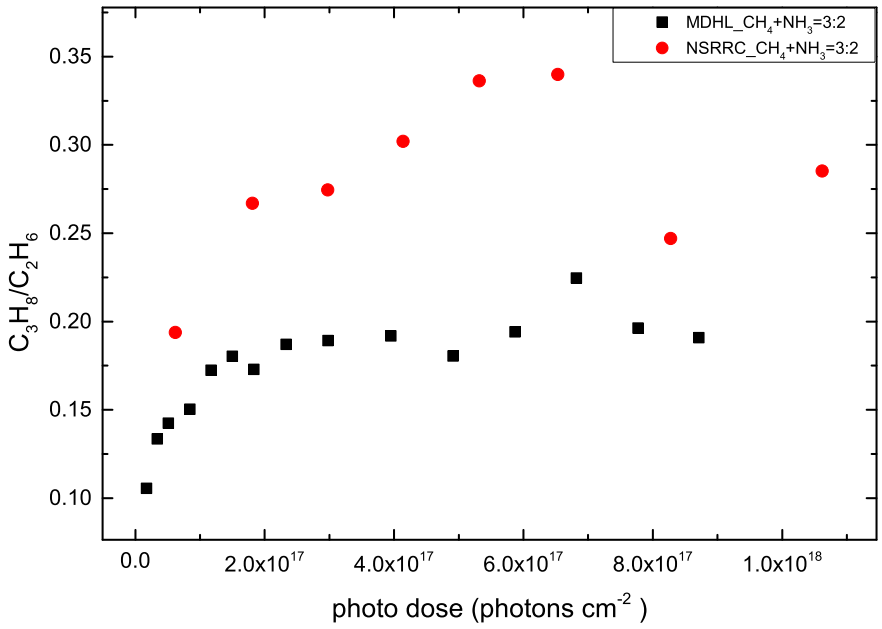

Figure 3.11: The column density of C_3H_8 divided by C_2H_6 accumulated when different configurations of CH_4 + NH_3 ice mixtures are irradiated by VUV and EUV photons

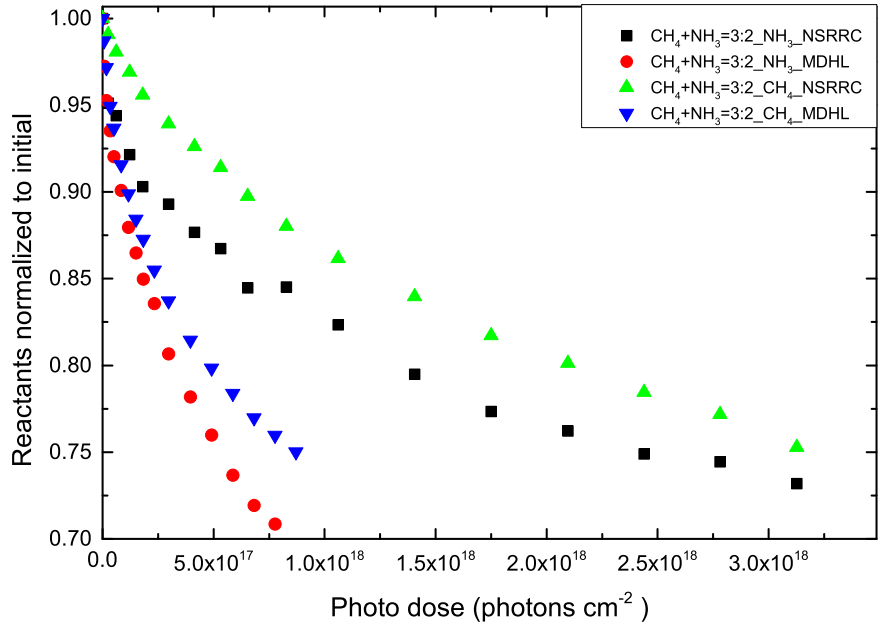

Figure 3.12: The normalized reduction of CH_4 and NH_3 in CH_4 + NH_3 ice mixtures irradiated by VUV and EUV photons

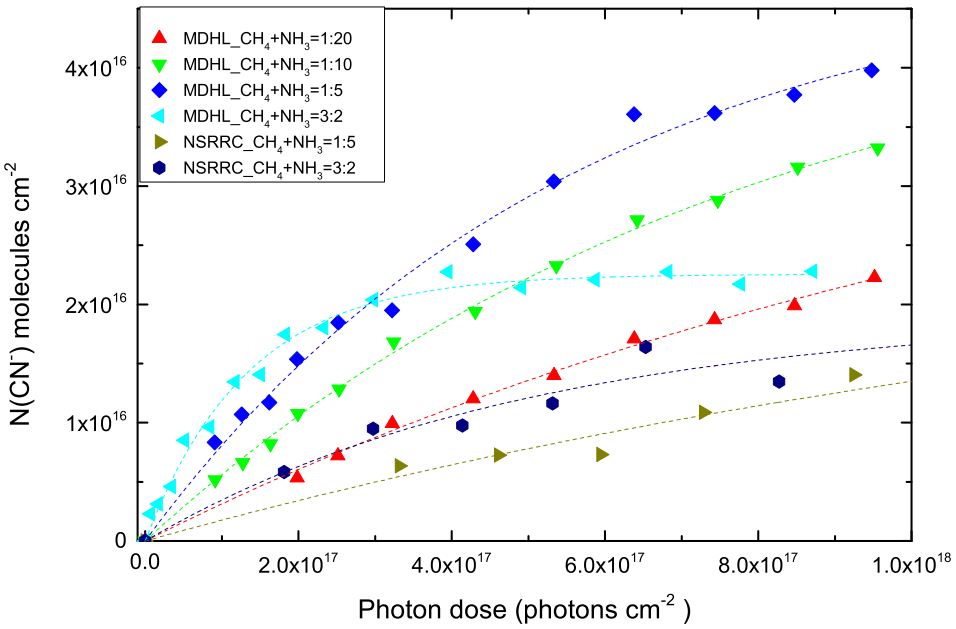

Figure 3.13: The column densities of CN^- generated by irradiation of CH4+NH3 ice mixtures by MDHL and 30.4 nm monochromatic light.

generated by irradiation of CH_4+NH_3 ice mixtures by MDHL and 30.4 nm monochromatic light. The fitting results are shown in Table 3.6. The rate constants forming CN^- is 3.06 to 4.13 times larger in CH_4+NH_3 = 1:5 and 3:2 irradiated by MDHL than irradiated by 30.4 nm monochromatic light respectively. Recall the CH_4 reduction in NSRRC is 6.06±0.07 times slower. With the rate constants of CN^- only 3.06 to 4.13 times smaller, the 6 times slower in CH_4 reduction and 3 times slower in CN^- formation give rise to a similarity of reduced NH_3 destruction cross-section and reduced rate in CN^- production in EUV irradiation experiments. Therefore, we may conclude that the reduction in CN^- formation rate by 30.4nm EUV irradiation is mainly due to the decreased NH_3 destruction cross-sections.

Table 3.6: The fitting results of CN^- by equation 2.10

Light source	Ratio of CH_4+NH_3	A (x10^{16} molecules cm^{-2})	k_1 (x10^{-18} $photon^{-1}$)	k_2 ($photon^{-1}$)
VUV	1:5	4.61 ± 0.18	1.93 ± 0.19	>1
	3:2	2.24 ± 0.03	8.21 ± 0.70	>1
EUV	1:5	2.89 ± 1.29	0.63 ± 0.37	>1
	3:2	2.24 ± 0.03	1.92 ± 1.99	>1

Fitting result of figure **??** with pseudo first order equation [CN-]=A(1-e-kx). These fitting results of MDHL experiments are an average of at least 2 experiments with the same circumstances. In the expression, A represents the column density when x, the photon dose, becomes infinitely large and k is the rate constant..


國立中央大學

Bibliography

[1] Donald E. Knuth. *The TEXbook, Volume A of Computers and Typesetting.* Addison-Wesley, Reading, Massachusetts, second edition, 1984, ISBN 0-201-13448-9.
http://www-cs-staff.stanford.edu/~knuth/index.html

[2] Leslie Lamport. *LaTeX: A Document Preparation System.* Addison-Wesley, Reading, Massachusetts, second edition, 1994, ISBN 0-201-52983-1.

[3] J. LO, *eThinking in Circuits with PSpice.* Cavesbooks, Inc., 2012, ISBN 978-957-41-8721-8.

[4] ——, *aThinking in Control with Matlab.* Cavesbooks, Inc., 2012, ISBN pending.

[5] ——, *LaTeX & U 自助出版.* 中央敦煌, 北科文具部, 2012, ISBN 978-957-41-9448-3.

[6] ——, *Packages author of ncuthesis(CJK, Xe), bizcard, cnwritingCJK.* Free packages, 2012.
https://code.google.com/p/ncu-thesis-latex-template/

[7] *Writing a thesis in LaTeX* http://texblog.org/

[8] Chinese character \cjk within \section{} does not work using pdflatex, + \includegraphics,
http://tex.stackexchange.com/a/126570

[9] *Page numbers only appear on pages where a chapter starts,*
http://tex.stackexchange.com/a/79776

國立中央大學
機械工程研究所

碩/博士論文 模版 ncuthesisCJK 使用說明

羅吉昌撰

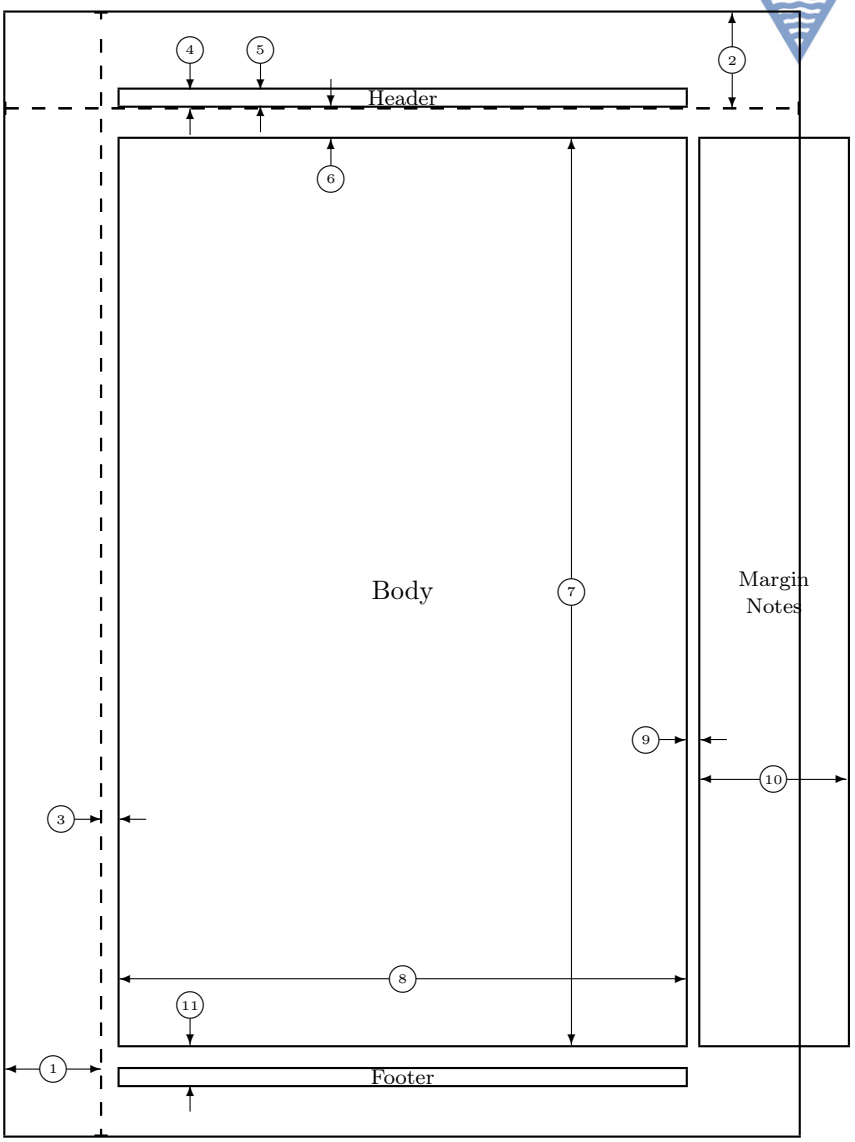

1	one inch + \hoffset	2	one inch + \voffset
3	\oddsidemargin = 14pt	4	\topmargin = -14pt
5	\headheight = 12pt	6	\headsep = 25pt
7	\textheight = 682pt	8	\textwidth = 426pt
9	\marginparsep = 11pt	10	\marginparwidth = 111pt
11	\footskip = 30pt		\marginparpush = 5pt (not shown)
	\hoffset = 0pt		\voffset = 0pt
	\paperwidth = 597pt		\paperheight = 845pt

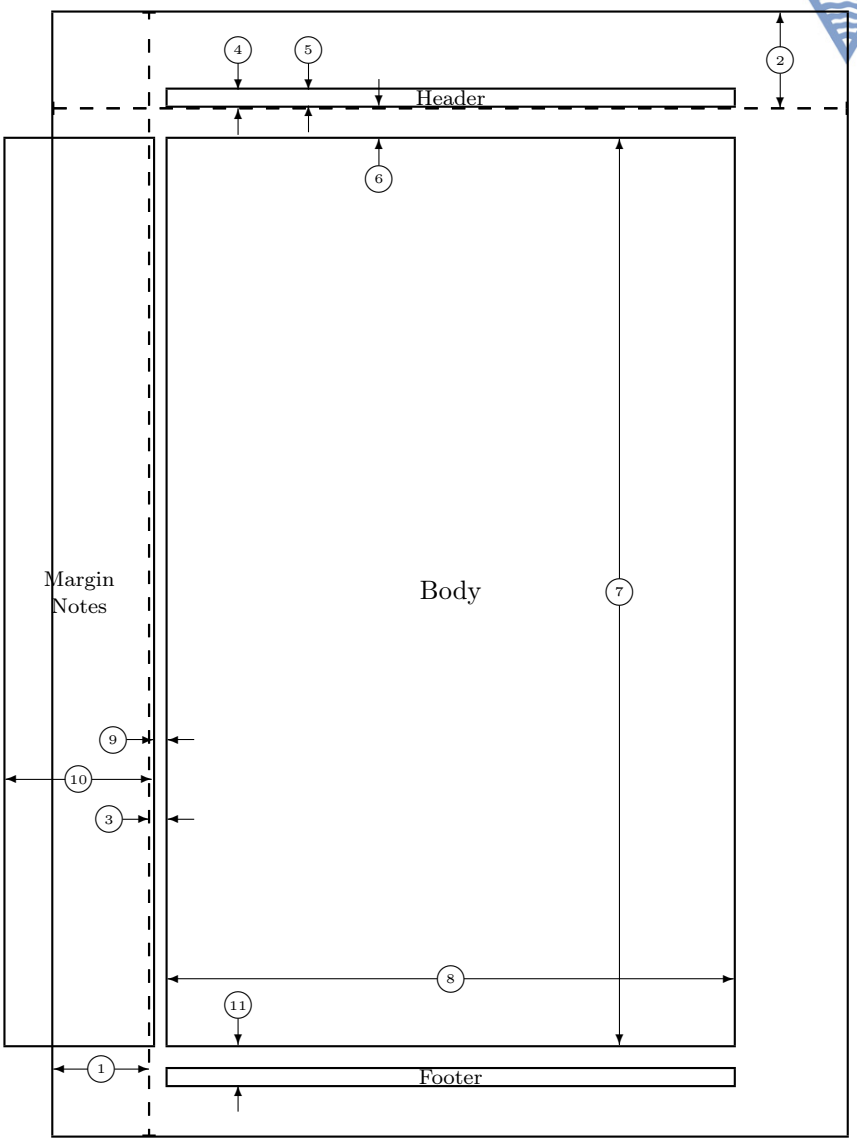

1	one inch + \hoffset	2	one inch + \voffset
3	\evensidemargin = 14pt	4	\topmargin = -14pt
5	\headheight = 12pt	6	\headsep = 25pt
7	\textheight = 682pt	8	\textwidth = 426pt
9	\marginparsep = 11pt	10	\marginparwidth = 111pt
11	\footskip = 30pt		\marginparpush = 5pt (not shown)
	\hoffset = 0pt		\voffset = 0pt
	\paperwidth = 597pt		\paperheight = 845pt